

# Quantifying Kinematic Substructure in the Milky Way's Stellar Halo

Xiang-Xiang Xue<sup>1,2</sup>, Hans-Walter Rix<sup>2</sup>, Brian Yanny<sup>3</sup>, Timothy C. Beers<sup>4</sup>, Eric F. Bell<sup>5,2</sup>, Gang Zhao<sup>1</sup>, James S. Bullock<sup>6</sup>, Kathryn V. Johnston<sup>7</sup>, Heather Morrison<sup>8</sup>, Constance Rockosi<sup>9</sup>, Sergey E. Koposov<sup>10,2,11</sup>, Xi Kang<sup>12,2</sup>, Chao Liu<sup>2</sup>, Ali Luo<sup>1</sup>, Young Sun Lee<sup>4</sup>, Benjamin. A. Weaver<sup>13</sup>

## ABSTRACT

We present and analyze the positions, distances, and radial velocities for over 4000 blue horizontal-branch (BHB) stars in the Milky Way's halo, drawn from SDSS DR8. We search for position-velocity substructure in these data, a signature of the hierarchical assembly of the stellar halo. Using a cumulative “close pair distribution” (CPD) as a statistic in the 4-dimensional space of sky position, distance, and velocity, we quantify the presence of position-velocity substructure at high statistical significance among the BHB stars: pairs of BHB stars that

---

<sup>1</sup>Key Lab of Optical Astronomy, National Astronomical Observatories, CAS, 20A Datun Road, Chaoyang District, 100012, Beijing, China

<sup>2</sup>Max-Planck-Institute for Astronomy Königstuhl 17, D-69117, Heidelberg, Germany

<sup>3</sup>Fermi National Accelerator Laboratory, P.O. Box 500 Batavia, IL 60510-5011, USA

<sup>4</sup>Department of Physics and Astronomy and JINA: Joint Institute for Nuclear Astrophysics, Michigan State University, E. Lansing, MI 48824, USA

<sup>5</sup>Department of Astronomy, University of Michigan, 500 Church Street, Ann Arbor, Michigan, 48109, USA

<sup>6</sup>Center for Cosmology, Department of Physics and Astronomy, University of California, Irvine, CA 92697, USA

<sup>7</sup>Astronomy Department, Columbia University, New York, NY 10027, USA

<sup>8</sup>Department of Astronomy, Case Western Reserve University, Cleveland, OH 44106, USA

<sup>9</sup>Lick Observatory/University of California, Santa Cruz, CA 95060, USA

<sup>10</sup>Institute of Astronomy, Madingley Road, Cambridge CB3 0HA, UK

<sup>11</sup>Sternberg Astronomical Institute, Universitetskiy pr. 13, 119992 Moscow, Russia

<sup>12</sup>Purple Mountain Observatory, CAS, 2 West Beijing Road, Nanjing, 210008, China

<sup>13</sup>Center for Cosmology and Particle Physics, New York University, New York, NY 10003, USA

are close in position on the sky tend to have more similar distances and radial velocities compared to a random sampling of these overall distributions. We make analogous mock-observations of 11 numerical halo formation simulations, in which the stellar halo is entirely composed of disrupted satellite debris, and find a level of substructure comparable to that seen in the actually observed BHB star sample. This result quantitatively confirms the hierarchical build-up of the stellar halo through a signature in phase (position-velocity) space. In detail, the structure present in the BHB stars is somewhat less prominent than that seen in most simulated halos, quite possibly because BHB stars represent an older sub-population. BHB stars located beyond 20 kpc from the Galactic center exhibit stronger substructure than at  $r_{\text{gc}} < 20$  kpc.

*Subject headings:* galaxies: individual(Milky Way) — Galaxy: halo — Galaxy: structure — stars: horizontal-branch — stars: kinematics and dynamics

## 1. Introduction

The current hierarchical structure formation paradigm implies that the formation of our Milky Way entailed a sequence of dark matter driven accretion and merger events (Searle & Zinn 1978; White & Rees 1978; Blumenthal et al. 1984). This naturally results in the expectation that the stellar halo should be largely built up from stars of tidally disrupted satellite galaxies, resulting in substructure that may appear as stellar streams with different degrees of phase-mixing (e.g. Bullock et al. 2001; Cooper et al. 2010b; Bullock & Johnston 2005, hereafter BJ05). Because stars are gravitationally collisionless systems, their phase-space (spatial and velocity) distributions encode and retain aspects of their origin. This implies that an analysis of substructure in the position-velocity distribution of stars in the halo is a direct test for hierarchical models of galaxy formation.

In the past decades, observational evidence of spatial substructure has indeed been found in the Milky Way, both near the Sun (Majewski et al. 1996; Helmi et al. 1999) and at larger distances (Ibata et al. 1994, 1995). The most prominent example is the discovery of the Sagittarius dwarf galaxy (Ibata et al. 1994, 1995; Yanny et al. 2000) and its trails of debris (Ibata et al. 2001; Majewski et al. 2003).

In nearby samples of stars, where the full 6D phase-space coordinates can be measured, substructure in the stellar distribution is seen in velocity space, or even in the integrals of motion (Dehnen & Binney 1998; Helmi et al. 1999; Klement et al. 2008, 2009; Morrison et al. 2009; Smith et al. 2009). At distances from the Sun characteristic of the stellar halo,

$\sim 20$  kpc, individual transverse velocities are all but impossible to measure from proper motions with current technology. The available observables are therefore the position in the sky, a distance estimate from photometric or spectroscopic luminosity determinations, and line-of-sight velocity:  $\alpha, \delta, d$ , and  $V_{los}$ . When averaged over large angular areas and broad distance ranges, the line-of-sight kinematics of the Milky Way halo stars at 10-50 kpc are well-described by a simple Gaussian with  $\sigma_{los} \approx 111 \text{ km s}^{-1}$  (Xue et al. 2008, hereafter X08). However, because the stellar halo is collisionless, preserving phase-space density, substructure in position space necessarily implies substructure in velocity space. Recent work by Starkenburg et al. (2009) and De Propris et al. (2010) indicate that the Milky Way’s stellar halo indeed possesses detectable position-velocity substructure. Schlafman et al. (2009) have shown that metal-poor halo stars within  $\sim 17.5$  kpc from the Sun exhibit clear evidence for velocity clustering on very small spatial scales (which the authors refer to as Elements of Cold Halo Substructure, or ECHOS).

With the development of large-scale sky surveys, such as the Two Micron All Sky Survey (2MASS; Skrutskie et al. 2006), the Sloan Digital Sky Survey (SDSS; York et al. 2000; Stoughton et al. 2002; Abazajian et al. 2003, 2004, 2005, 2009; Adelman-McCarthy et al. 2006, 2007, 2008), and the follow-up SEGUE survey (Yanny et al. 2009b), we have an unprecedented opportunity to examine Milky Way halo streams in detail (Ivezić et al. 2000; Yanny et al. 2000; Newberg et al. 2002; Majewski et al. 2003; Yanny et al. 2003; Newberg et al. 2007; Yanny et al. 2009a). Halo star samples are now of sufficient size and quality that a direct statistical comparison with models, such as BJ05, has become possible.

A first quantitative comparison indicated that the observed level of *spatial* substructure (on all scales) is similar to that expected from those simulations, where the halo is composed entirely of disrupted satellites (Bell et al. 2008, hereafter B08). Imaging surveys of M31 (Ibata et al. 2007) have revealed a similarly rich set of substructure in the stellar halo of that galaxy. Based on photometry of main sequence turn-off (MSTO) stars, B08 constructed a coarse 3D map of the stellar halo density, with almost a factor of two uncertainty in distances. BHB stars are a much rarer tracer of the old metal-poor population, but have the great advantage of being luminous, with  $M_g \sim +0.7$  (vs.  $M_g \sim 3.5$  for MSTO stars) and of having precise distance estimates ( $\sim 5\%$ ; X08). BHB stars have also been a special spectroscopic target class in SDSS and SEGUE (e.g., Yanny et al. 2009b). Hence, the sample of possible BHB stars with spectra from SDSS constitutes by far the largest set of luminous tracers (extending to distances of  $\sim 80$  kpc) of the Milky Way’s stellar halo with available four dimensional ( $\alpha, \delta, d, V_{los}$ ) information, where the distances are accurate to 5% and the radial velocities accurate to  $5 \sim 20 \text{ km s}^{-1}$ . This sample enables the first attempt at checking that the statistical properties of kinematics matches (or not) model expectations.

This paper describes a large sample of probable BHB stars with measured kinematics, and presents an exploration of how to quantify position-velocity substructure in the Milky Way’s stellar halo in order to compare the observation to simulations such as from BJ05. It is certainly possible to pick out the kinematic signature of the Sagittarius stream (e.g., Ibata et al. 2001; Starkenburg et al. 2009) in these data. However, what we aim for here is to devise a simple objective measure for quantifying such substructure. Specifically, we employ the close pair distribution (CPD) statistic,  $F = w_\theta \theta^2 + w_{\Delta d} (\Delta d)^2 + w_{\Delta V_{los}} (\Delta V_{los})^2$ , to detect substructure, following Starkenburg et al. (2009). Here,  $\theta$ ,  $\Delta d$ ,  $\Delta V_{los}$  are the angular, distance, and velocity separation of pairs of stars, and  $w_\theta$ ,  $w_{\Delta d}$ , and  $w_{\Delta V_{los}}$  are suitable weights. The idea is that a structured or “clumpy” position-velocity distribution will have more pairs with small F than a suitably chosen random distribution. As also argued by B08, it is important for quantitative data-model comparisons to have a general statistical measure of substructure, rather than specifically searching for (here, kinematical) substructure associated with a particular feature, such as the Sagittarius stream, so we also explore what we should expect from the BJ05 models, and compare with the observations.

This paper is organized as follows. In Section 2 we present the sample of BHB stars. Section 3 provides the definition of the close pair distribution (CPD) as a statistic, and describes its application to the sample of BHB stars. The analogous CPD for the BJ05 simulations and their statistical analysis is presented in Section 4. Conclusions from the comparisons between observations and simulations are presented in Section 5.

## 2. The Spectroscopic Sample of BHB stars from SDSS DR8

SDSS-I was an imaging and spectroscopic survey that began routine operations in April 2000, and continued through June 2005. The SDSS and its extensions are using a dedicated 2.5m telescope (Gunn et al. 2006) located at the Apache Point Observatory in New Mexico. The Sloan Extension for Galactic Understanding and Exploration (SEGUE) is one of the three key projects (the legacy survey, the supernova survey, and SEGUE) in the recently completed first extension of the Sloan Digital Sky Survey, known collectively as SDSS-II. The SEGUE program, which ran from July 2005 to July 2008, obtained *ugriz* imaging of some 3500 deg<sup>2</sup> of sky outside of the SDSS-I footprint (Fukugita et al. 1996; Gunn et al. 1998, 2006; York et al. 2000; Hogg et al. 2001; Smith et al. 2002; Stoughton et al. 2002; Abazajian et al. 2003, 2004, 2005, 2009; Pier et al. 2003; Ivezić et al. 2004; Adelman-McCarthy et al. 2006, 2007, 2008; Tucker et al. 2006), with special attention being given to scans of lower Galactic latitudes ( $|b| < 35^\circ$ ) in order to better probe the disk/halo interface of the Milky Way. SEGUE obtained some 240,000 medium-resolution spectra of stars in the Galaxy, selected

to explore the nature of stellar populations from 0.5 kpc to 100 kpc (Yanny et al. 2009b). SDSS-III, which is presently underway, has already completed the sub-survey SEGUE-2, an extension intended to obtain an additional sample of over 120,000 spectra for distant stars that are likely to be members of the outer-halo population of the Galaxy. Data from SEGUE-2 has been distribution as part of the eighth public data release, DR8 (Aihara et al. 2011).

The SEGUE Stellar Parameter Pipeline processes the wavelength- and flux-calibrated spectra generated by the standard SDSS spectroscopic reduction pipeline (Stoughton et al. 2002), obtains equivalent widths and/or line indices for more than 80 atomic or molecular absorption lines, and estimates  $T_{\text{eff}}$ ,  $\log g$ , and  $[\text{Fe}/\text{H}]$  through the application of a number of approaches (see Lee et al. 2008a,b; Allende Prieto et al. 2008; Smolinski et al. 2011).

We construct a sample of BHB stars from SDSS DR8 with spectra in a fashion very similar to X08. The spectra are used both to classify stars as BHB and to obtain measured radial velocities. In essence, we combine an initial color cut for BHB candidates with Balmer-line profile shape measurements. The S/N of the spectra affects the precision of Balmer-line profile shape measurements. Therefore, spectra are only accepted when the fractional variance between the best-fitting profile and observed Balmer-line profile is  $\leq 0.1$ . The color cuts that we used in this paper are:

$$\begin{aligned} 0.8 < u - g < 1.5 \\ -0.5 < g - r < 0.0 \end{aligned}$$

The Balmer-line profile cuts used are:

$$\text{for the H}\delta \text{ line : } \quad D_{0.2} \leq 29 \text{ \AA}, \quad f_m \leq 0.35$$

$$\text{for the H}\gamma \text{ line : } \quad 0.75 \leq c_\gamma \leq 1.25, \quad 7 \text{ \AA} \leq b_\gamma \leq 10.8 - 26.5 (c_\gamma - 1.08)^2$$

where  $D_{0.2}$ ,  $f_m$ ,  $c$ , and  $b$  are the width of the Balmer line at 20% below the local continuum, the flux relative to the continuum at the line core, and the parameters of the Sérsic profile,  $y = 1.0 - a \exp \left[ - \left( \frac{|\lambda - \lambda_0|}{b} \right)^c \right]$ , respectively (see Sirko et al. 2004, X08).

The following are the Balmer-line profile cuts used in X08:

$$\text{for the H}\delta \text{ line : } \quad 17 \text{ \AA} \leq D_{0.2} \leq 28.5 \text{ \AA}, \quad 0.1 \leq f_m \leq 0.3$$

$$\text{for the H}\gamma \text{ line : } \quad 0.75 \leq c_\gamma \leq 1.25, \quad 7 \text{ \AA} \leq b_\gamma \leq 10.8 - 26.5 (c_\gamma - 1.08)^2$$

We retain the color cut (Yanny et al. 2000), but slightly relax the Balmer-line profile cuts compared to X08, as illustrated in Figure 1. Since the two Balmer-line profile cuts

are independent, the relaxed criteria on the  $H\delta$  line should introduce little additional contamination, but overall it makes the criteria less stringent. As compared with our previous criteria (X08), the relaxed criteria will have minimal impact on the following substructure analysis. For further details on the sample selection, we refer the interested reader to X08 and references therein.

By selecting stars that satisfy the color cuts and both Balmer-line profile cuts, we obtain a sample of 4985 stars from SDSS DR8 with high BHB probability (see Table 1 for example), of which there are 4625 halo BHB stars with  $|Z| > 4$  kpc and  $r_{gc} < 60$  kpc and 26 halo BHB stars between 60 and 80 kpc. Figure 2 shows the sky coverage and spatial distribution of these 4625 halo BHB stars. Distances were derived from the magnitudes and colors as in X08. The line-of-sight velocities,  $V_{los}$ , are converted from Local Standard of Rest frame to the Galactic Standard of Rest frame by adopting a value of  $220 \text{ km s}^{-1}$  for the Local Standard of Rest ( $V_{lsr}$ ) and a solar motion of  $(+10.0, +5.2, +7.2) \text{ km s}^{-1}$ , as in X08. Small changes that may arise from adopting a different  $V_{cir}(R_0)$  pair, e.g., Bovy et al. (2009) or Koposov et al. (2010), do not matter for the subsequent analysis.

This sample of halo BHB stars has radial velocity errors of 5-20  $\text{km s}^{-1}$  and much more accurate distances than other distant halo stars with available kinematic information. For instance, distances are  $\sim 4\times$  more accurate than in the sample of halo giants recently used by Starkenburg et al. (2009) in a search for distant halo substructure, and our sample is 50-fold larger. Schlafman et al. (2009) discussed a sample of  $\sim 10,000$  metal-poor main sequence turnoff (MPMSTO) stars with distances greater than 10 kpc from the Galactic center, with vertical distance  $|Z|$  more than 4 kpc, and with distances less than 17.5 kpc from the Sun, to identify ECHOS in the inner halo. By comparison, our sample extends to four times larger distance.

The cumulative distribution of the BHB stars with  $r_{gc}$  shown in Figure 3 indicates that about 95% of the BHB stars have  $r_{gc} \leq 40$  kpc, so that any estimate of substructure should be dominated by the BHB stars within this distance. For a cleaner selection function, we use only the 4243 BHB stars with  $|Z| > 4$  kpc and  $r_{gc} \leq 40$  kpc in the following analysis, which is still sufficiently distant to enable tests for substructure well into the outer halo.

### 3. The Close Pair Distribution of BHB stars in DR8

We now turn to quantifying the presence of any kinematic substructure. There is no unique choice of a substructure statistic, nor is there a rigorous way to derive one without making very specific assumptions about the nature of the underlying distributions. For

kinematically cold streams that are not strongly phase-mixed, a “pairwise velocity difference” (PVD),  $\langle |\Delta V_{los}| \rangle (\Delta r_{gc}^{\vec{}})$ , could conceivably be used to detect velocity substructure. It is expected that  $\langle |\Delta V_{los}| \rangle$  should be lower for small separations  $\Delta r_{gc}^{\vec{}}$  in stellar streams, where adjacent stars have similar velocities. However, as many streams in simulated halos are phase-wrapped, the PVD proved not to be very suitable to quantify substructure, even in simulated halos where all stars arise from disrupted satellites (see Xue et al. 2009).

For distant large scale features, a great circle method (Lynden-Bell & Lynden-Bell 1995; Palma et al. 2002) may be appropriate. We have chosen not to use such a method in this paper for two reasons. Most importantly, BJ05 and Johnston et al. (2008) demonstrate that many halo structures (in particular older structures or those on more radial orbits) do not have a great circle geometry, and we wish to explore the degree of halo structure in a way that is sensitive in principle to a broader range of geometries. Secondly, the spectroscopic coverage is sparse and covers only a fraction of the sky, and we lack useful proper motion information for our sample, making a great circle analysis more challenging to implement.

As an alternative to the PVD and a great circle analysis, we follow Starkenburg et al. (2009) and De Propris et al. (2010) in exploring a statistic that focuses on the incidence of close pairs in  $(\alpha, \delta, d, V_{los})$  space (a similar approach was developed by Doinidis & Beers 1989). Specifically, we define the separation between two stars  $i$  and  $j$  as:

$$F_{ij} = w_{\theta} \theta_{ij}^2 + w_{\Delta d} (d_i - d_j)^2 + w_{\Delta V_{los}} (V_{los,i} - V_{los,j})^2 \quad (1)$$

where

$$\begin{aligned} \cos \theta_{ij} &= \cos b_i \cos b_j \cos(l_i - l_j) + \sin b_i \sin b_j, \\ w_{\theta} &= \frac{1}{\langle \theta^2 \rangle}, w_{\Delta d} = \frac{1}{\langle (\Delta d)^2 \rangle}, w_{\Delta V_{los}} = \frac{1}{\langle (\Delta V_{los})^2 \rangle}; \end{aligned}$$

and where  $\langle \dots \rangle$  refers to the average over all pairs.

While the angular separation combines the galactic longitude and latitude in the distance measure  $F$ , the heliocentric distance and line-of-sight velocity are used as independent variables... . In the definition of  $F$ , the weights  $w_{\theta}$ ;  $w_{\Delta d}$ ;  $w_{\Delta V_{los}}$ , are solely used to create a consistent metric for the angular, distance and velocity dimensions of  $F$  through normalizing each dimension by the ensemble average of separation, ( $\langle \theta^2 \rangle = 6928$  squaredegree), distance difference ( $\langle (\Delta d)^2 \rangle = 127 \text{ kpc}^2$ ), line-of-sight velocity difference ( $\langle (\Delta V_{los})^2 \rangle = 22455 \text{ km}^2\text{s}^{-2}$ ). Starkenburg et al. (2009) have pointed out that this algorithm is quite insensitive to small changes in the weighting factors. We use somewhat different weighting factors from them, but still detect obvious substructure signal in the BHB sample presented here. In parallel work to this paper Cooper et al. (2010a) applied the algorithm and weighting factors as Starken-

burg et al. (2009) to 2400 BHB stars and found obvious substructure signal. Therefore, the choice of weighting factors seems not to be a critical aspect of sub-structure quantification.

If position-velocity substructure is present, we expect that the distribution of  $F_{ij}$  for the observed sample has more close pairs than the null hypothesis (defined below) of a smooth halo where positions and velocities are uncorrelated:  $N_{obs}(< F) > N(< F_0)$ . This is most conveniently captured in the cumulative distribution of the  $F_{ij}$ ,  $N(< F)$ , as illustrated in Figure 4.

This null hypothesis assumes that the halo can be described by some spatial density distribution,  $\rho_{BHB}(\vec{r})$ , and a velocity distribution where  $\sigma_{los}$  does not depend on the particular position. Indeed, averaged over all angles,  $\sigma_{los} \approx 111 \text{ km s}^{-1}$  is observed to be nearly constant as a function of radius (X08). In its angular distribution and its distance distribution, the sample selection function of our BHB sample is very complex (see, e.g., Figure 2 for the angular distribution). However, stellar radial velocities are uncorrelated to the sample selection, and it is reasonable to assume that the distance selection of the stars in the same part of the sky are independent realizations of the overall distance (or, apparent magnitude) distribution. Consequently, we cannot randomize  $\theta$  when constructing the null hypotheses. As our null hypothesis, we can only independently draw random  $\Delta d$  and  $\Delta V_{los}$ . Specifically, we do this by scrambling *only* the distances and velocities within the sample to create the null hypothesis, but leave the angular position unchanged:

$$F_{0,ij} = w_{\theta}\theta_{ij}^2 + w_d(d_{i_r} - d_{j_r})^2 + w_{V_{los}}(V_{los,i_r} - V_{los,j_r})^2, \quad (2)$$

where  $w_{\theta}$ ,  $w_d$ ,  $w_{V_{los}}$ , and the indices  $i$  and  $j$  are exactly the same as in  $F_{ij}$ , but  $i_r$  and  $j_r$  are random indices chosen within an angle<sup>1</sup> of  $45^\circ$  from stars  $i$  and  $j$  (here,  $i_r$  and  $j_r$  are different and independent in their distance and velocity terms).

Now we can search for position-velocity substructure by comparing  $N_{obs}(< F)$  for our BHB sample to the distribution of 100 Monte Carlo representations of  $N(< F_0)$ . Figure 4 shows that  $N_{obs}(< F)$  exceeds  $N(< F_0)$  at high significance for small  $F$ ,  $\log F < -2$  (for example,  $\Delta d < 1.5 \text{ kpc}$ ,  $\Delta V_{los} < 15 \text{ km s}^{-1}$  and  $\theta < 8^\circ$  corresponds to  $\log F < -2$ ).

Small values of  $F$  represent close pairs in position-velocity space. So, Figure 4 demonstrates that the observed sample has many more close pairs than the null hypothesis, reflecting the existence of position-velocity substructure in the BHB sample. For small  $F$  one might

---

<sup>1</sup>Angular spacing comparable to or larger than the SDSS footprint may be hard to interpret, so we choose  $45^\circ$  to avoid this.



expect  $N(< F_0) \propto F_0^2$  for the null hypothesis, but the plot shows a somewhat shallower slope, presumably arising from the non-random way that stars are sampled by SDSS spectroscopy from the celestial sphere. The widely spaced SEGUE-1/2 spectroscopic plates result in the sparse, but locally dense, angular sampling. In addition, we can learn from Figure 4 that the CPD statistic focuses on  $< 0.1\%$  close pairs rather than all pairs of the sample, implying that the CPD may be more sensitive to the presence of substructure than the PVD statistic (see Xue et al. 2009).

The left panel of Figure 4 shows that there are only 30 pairs with  $\log F < -3$ , compared with total pairs of  $8.9 \times 10^6$ . Therefore, we just analyze the behavior at  $\log F > -3$  in the subsequent analysis.

As shown in Figure 5, the substructure signal comes both from the distance and the line-of-sight velocity domain. This is apparent if we either scramble *only* the distances or *only* the velocities between  $N_{obs}(< F)$  and  $N(< F_0)$ . In both cases an excess of small separation pairs is present at a comparable level.

The recent studies of Carollo et al. (2007) and Carollo et al. (2010), based on local samples of halo stars, indicate that our Milky Way’s stellar halo is complex, and can be described by at least two components – denoted as an “inner” and an “outer” halo, with different kinematics, distributions of orbital eccentricity, inferred spatial profiles, and peak metallicities. In such a decomposition, the inner halo component dominates the region of  $5 \text{ kpc} < r_{gc} < 10 \text{ kpc}$ , while the region of  $r_{gc} > 20 \text{ kpc}$  is dominated by the outer halo. Direct in situ evidence for stellar metallicity changes with distance has also been found in photometry from the SEGUE vertical stripes (de Jong et al. 2010).

As dynamical timescales are longer at large distances, we would expect a more clear substructure signal in the outer parts of the halo. To test this, we include here the BHB stars with  $40 \text{ kpc} < r_{gc} < 60 \text{ kpc}$ . We divide the BHB sample into two parts – subsample I with  $5 \text{ kpc} < r_{gc} < 20 \text{ kpc}$ , and subsample II with  $20 \text{ kpc} < r_{gc} < 60 \text{ kpc}$ , both with  $|Z| > 4 \text{ kpc}$ , and compare the substructure signals in the two subsamples. Figure 6 shows that both show significant deviations from the null hypothesis. Yet, subsample II shows a stronger clustering excess in 4D space than subsample I. This suggests that the substructure is stronger (e.g. less phase-mixed) in the outer halo (subsample II) than in the inner halo (subsample I).

As mentioned in the introduction, we are more interested in a general statistical measure of substructure for quantitative data-model comparison than in the search for substructure associated with a particular feature;  $N(< F)$  appears as a useful statistic in this context.

#### 4. Position-Velocity Substructure in the BJ05 Models

Having detected a general substructure signal, we now compare this to expectations for  $N(<F)$  from cosmological models where the entire stellar halo is made of disrupted satellite galaxies.

BJ05 published models for the formation of the stellar halo of the Milky Way system, arising solely from the accretion of  $\sim 100 - 200$  luminous satellite galaxies in the past  $\sim 12$  Gyr. They used a hybrid semi-analytic plus N-body approach that distinguished explicitly between the evolution of baryonic matter and dark matter in accreted satellites. For further details of the simulations, we refer the interested reader to BJ05, Robertson et al. (2005), Font et al. (2006), and references therein. There are 11 simulated halos provided by the Bullock & Johnston study, which can be obtained from <http://www.astro.columbia.edu/~kvj/halos/>. The simulations produce a realistic stellar halo, with mass and density profiles much like that of the Milky Way (e.g. B08), and with surviving satellites matching the observed number counts and structural parameter distributions of the satellite galaxies of the Milky Way. Sharma et al. (2011) published a code to generate a synthetic survey of the Milky Way based on BJ05 simulations. Given one or more color-magnitude bounds, a survey size, and geometry, this code can return a catalog of stars in accordance with a given model of the Milky Way. The Galaxia code will be released publicly at <http://galaxia.sourceforge.net>. We refer the interested reader to Sharma et al. (2011) and references therein.

To start, we assume that BHB stars are representative tracers of the overall population of old, metal-poor, halo stars (see, however, Bell et al. 2010). We then make “mock-observations” of the BJ05 simulations, analogous to those presented in Section 2 and analyzed in Section 3. In brief, we do this by accounting for the particular survey volume of SDSS DR8, the angular separation distribution, and approximate distance distribution of the BHB sample, accounting for the luminosity weight of the simulated particles, and by adding observational uncertainties for distance and velocity.

From the simulations, we obtain the particle’s 3D positions and 3D velocities in the Galactic standard of rest frame, luminosities  $L$ , and ages. We transfer these to Galactocentric line-of-sight velocities,  $V_{los}$ , and sky positions (Galactic longitude and latitude,  $(l, b)$ ), by taking the Sun’s position as  $(8.0, 0.0)$  kpc. The probability of a particle being drawn is proportional to the assigned particle luminosity. The SDSS fibers cannot be placed closer than about 55 arcsec. However, BHB stars are relatively sparse on the sky  $\sim 1$  per square degree, so possible fiber collisions play no role in the clustering analysis. E.g. fewer than  $10^{-5}$  of all possible pairwise angular separations in the sample fall within  $< 1'$ . We also consider the spectroscopic sky coverage of SDSS DR8, distance limits ( $|Z| \geq 4$  kpc,  $r_{gc} \leq 40$  kpc), and the angular separation distribution of the observations. These procedures essentially follow

those used by X08.

Based on the particles with the same sky coverage as SDSS DR8 and the same distance limits as the BHB sample, we randomly select a particle within an angle <sup>2</sup> of  $1.2^\circ$  from each BHB star  $i$  in the sample (where  $i = 1\dots 4243$ ). This selected particle of luminosity  $L$  is accepted with a probability of  $\leq L/L_{max}$ , where  $L_{max}$  is the maximum luminosity of the simulated particles. We also convolve the distances of the mock-observations with an error of 5%; the radial velocities are convolved with a Gaussian error of  $\sigma = 5 \text{ km s}^{-1}$ .

This procedure results in mock-observations of 4243 star particles in the simulations that are in the same sky region as SDSS DR8, have a similar angular separation distribution to the BHB sample, have the same distance and velocity uncertainties as the BHB sample, and have distance limits of  $|Z| \geq 4 \text{ kpc}$ ,  $r_{gc} \leq 40 \text{ kpc}$ , and satisfy the luminosity weighting scheme. The spatial distributions for 11 mock-observations are shown in Figure 7, along with the spatial distribution for BHB sample. These mock-observations allow us to consider the CPD for the BJ05 simulations. We calculate  $F$  for the mock-observations and 100 sets of the null hypothesis,  $F_0$ , in each of the 11 simulations.

The upper panel of Figure 8 shows the close pair distribution for the observed BHB sample and the 11 mock-observations. Overall, the observations fall well within the range of expectation from the BJ05 simulations, but the simulations have somewhat more substructure in the realm  $\log F \sim -2.5$  to  $-1$ . The ratio of the cumulative distribution of the mock-observations for all 11 simulated halos of BJ05 are shown in lower panel of Figure 8, along with the ratio of the cumulative distribution of the actual data. Inspection of this Figure reveals that  $N_{obs}(< F)$  differs significantly from  $N(< F_0)$  for all halos, in the sense that  $N_{obs}(< F) > N_{null}(< F)$  at least for  $< 1\%$  of closest pairs. The strength of the CPD signature varies quite strongly among different simulations. Overall, the ensemble of simulations show qualitatively the same signature of position-velocity substructure as seen in the real data. Moreover, the large majority of simulations exhibit stronger signals than observation for  $-3 < \log F < -1$  (except 2 BJ05 halos shown as lower panel of Figure 8). In particular, a significant substructure signal can be traced in the mock-observations to  $\log F \sim -1$  (e.g.,  $\Delta d < 4.5 \text{ kpc}$ ,  $\Delta V_{los} < 65 \text{ km s}^{-1}$ , and  $\theta < 26^\circ$  for  $\log F < -1$ ) for most of the simulations, while for the observations the substructure signal can only be traced until  $\log F \sim -2$ . This indicates some quantitative data-model difference.

The BHB sample qualitatively exhibits the same signature of position-velocity substructure as the BJ05 halos, which are by construction 100% substructured. This implies that a

---

<sup>2</sup>The  $1.2^\circ$  angular distance was found to be the smallest angle that can ensure there is at least one particle that can be accepted around star  $i$ .

large fraction of the Milky Way halo is associated with substructure. However, it is difficult to quantify the fraction of BHB stars in the Milky Way that are in substructures, because the variation among different all-substructure simulations is so large. At any rate, it has to be a substantial fraction.

Taken at face value, the tendency of the overall stellar halo of cosmologically-motivated models to have exhibit more substructure than observed BHB stars, may indicate that the models with their rigid halos may somewhat overpredict the degree of substructure; or this comparison may imply that some fraction of the Milky Way’s halo stars did indeed form in an early dissipational component (Hammer et al. 2007; Shen et al. 2010).

An alternative explanation may be this possibility, and noting that BHB stars do not fairly trace the overall halo star populations. To test that BHB stars occur in very old, metal poor populations, and we have tested if older star particles from the BJ05 simulation are distributed differently from all particles. To explore why the models might be somewhat more highly structured, especially for larger  $F$ , we compare the  $F$  distributions for the observation and the particles older than 11 Gyr in the BJ05 halos, where the age refers to the formation of the star particle, not the time since disruption of its host satellite. Figure 9 shows that the observed substructure signal is comparable with those detected in simulations (Except for 2 BJ05 halos). BHB stars are known to represent a very old population, so this may be an astrophysically reasonable explanation for the data-model difference.

Another possibility is that, since the models do not follow mergers self-consistently (i.e., the Milky Way’s potential grows only smoothly and analytically), the response of the Milky Way to infalling objects could serve to disrupt and scatter streams, thereby decreasing the importance of substructure. This could be checked in the future with simulations such as Cooper et al. (2010b).

As in the analysis of the BHB sample, we also make mock-observations of the inner- and outer-halo regions (here, the mock-observations have similar sky densities to the BHB sample), and calculate  $F$  and  $F_0$  for the mock-observations. Figure 10 shows that, for most BJ05 halos (except halo08), the outer halo ( $20 \text{ kpc} < r_{\text{gc}} < 60 \text{ kpc}$ ) exhibits a stronger substructure signal than the inner halo ( $5 \text{ kpc} < r_{\text{gc}} < 20 \text{ kpc}$ ), consistent with the actual observations.

The mock-observations show that the CPD deviates from the null hypothesis in the simulations in a qualitatively similar fashion as the actual observations. At first sight, this seems to be a straightforward extension into the kinematic domain of the conclusion reached by B08, that the stellar halo exhibits a level of substructure consistent with the stream-only

models of BJ05.<sup>3</sup> The signal is, however, weaker than that seen in mock-observations drawn from the BJ05 simulations.

Taken together, Figure 4, Figure 7, Figure 8, Figure 9 and Figure 10 lead to our four results: 1) In a sample of  $> 4000$  BHB stars from SDSS DR8 there is a very clear signal for position-velocity substructure in the Milky Way’s halo stars – close angular pairs of stars have smaller velocity and/or distance differences than expected for an uncorrelated distribution. 2) The outer part of the Milky Way’s halo ( $r_{gc} > 20$  kpc) exhibits a statistically stronger kinematic substructure signal than the inner halo ( $r_{gc} \leq 20$  kpc). 3) Mock-observations of simulated halos BJ05, made exclusively from disrupted satellites, exhibit a qualitatively very similar behavior –  $N_{\text{obs}}(< F) > N(< F_0)$  for  $\log F \leq -1$ . 4) Quantitatively, most simulations produce a stronger signal, especially one extending to larger scales (i.e., larger  $F$ ). However, if we identify BHB stars within the simulated halo population with  $t_{age} > 11$  Gyr, the levels of substructure are consistent. Given other evidence that BHB stars are most abundant in very old populations, this seems perhaps astrophysically more plausible than the alternative of postulating a very quiet formation of the Milky Way’s halo.

## 5. Summary and Conclusions

In the context of current cosmogonic models, the stellar halos of galaxies like our Milky Way are expected to be comprised, to a large degree, of debris from disrupted satellite galaxies. After disruption, the dispersing stars will form recognizable streams for some time, but may eventually phase-mix beyond easy recognition. There has been recent evidence (B08) that the degree of spatial substructure actually seen in the Milky Way’s halo matches that of simulations (e.g., BJ05), where the stellar halo arises exclusively from disrupted satellites. Due to phase-space conservation, the same scenario qualitatively predicts the existence of a position-velocity correlation. In this paper, we have pursued a quantitative statistical approach to understanding how the Milky Way’s stellar halo compares with this scenario.

It has already been established in the published literature that several prominent substructures exist in the Milky Way’s stellar halo, most notably the Sagittarius stream. The next step forward is to find simple, robust statistical measures to quantify the level of substructure in order to allow direct comparison with theoretical models (such as BJ05). There is certainly no established procedure, and there may be no unique way to establish such a

---

<sup>3</sup>In Bell et al. (2008) the BJ05 models are labeled 1-11 in strict numerical order, so that the interested reader can compare B08 and this paper side-by-side.

statistic. For example, in pure position space, B08 simply took the *rms* deviation of the density from a underlying power-law model. In this paper we have considered a statistic for diagnosing position-velocity correlations – the close pair distribution (see Starkenburg et al. 2009).

Building on recent initial attempts (Starkenburg et al. 2009; Xue et al. 2009; Harrigan et al. 2010; De Propris et al. 2010), this paper presented a more comprehensive attempt to quantify the position-velocity substructure of the Milky Way’s stellar halo, using BHB stars from SDSS, and to compare it to cosmological models. We calculated the close pair distribution (CPD) as a function of distance separation, angular separation, and velocity separation between pairs of stars. Qualitatively, the signal we were looking for is that the observations have significantly more close pairs than an ensemble of null hypotheses, where the position and velocity have no correlation. Using this CPD (i.e., the cumulative distribution  $N_{\text{obs}}(< F)$ , where  $F$  is the four-distance in angle, distance, and velocity), we found that a sample of over 4000 BHB stars in the halo of the Galaxy exhibit far more close pairs than the null hypothesis, which demonstrates the existence of real substructure. This result is perhaps not surprising, as some level of substructure is already known to exist (see also Starkenburg et al. 2009; De Propris et al. 2010; Harrigan et al. 2010). However, as a statistical quantification, it draws on a sample 6-60 times larger than previous analyses (Starkenburg et al. 2009; De Propris et al. 2010), and arrives at statistically very clear-cut inferences. We also constructed mock-observations of simulated stellar halos that are made exclusively of disrupted satellite galaxies. These mock-observations match the angular sampling of the SDSS data in detail, and also match the distance cuts applied to the data. Comparing, analogously,  $N_{\text{obs}}(< F)$  to  $N(< F_0)$ , we found the qualitatively same signature of substructure as in the observed sample. Quantitatively, the observed signal is weaker than that seen in the mock-observations, where the stellar halo is entirely made of disrupted satellites. Assuming that BHB stars are random tracers of the stars in the simulations, we impose a lower age limit of 11 Gyr in producing mock-observations, and found comparable levels of position-velocity substructure between observation and simulations. Therefore, there are two ways to reconcile the data-model differences: either to infer differences in the dynamical formation histories between the simulated and the observed Milky Way, or - more plausible in our view - attributing it to the fact that BHB stars are overrepresented in the oldest sub-populations of the stellar halo. For both the observations and the mock-observations we compared the substructure signals associated with the inner and outer halos, and found good agreement between data and model – the outer halo exhibits a stronger substructure signal than the inner halo.

Within the context of SDSS data, the next level of understanding kinematic substructure in the Milky Way’s outer halo will come from samples of more representative giant stars with

good distances. How the results from BHB stars presented here relate to the substructure seen in main-sequence samples of the inner halo (Schlaufman et al. 2009, ECHOS) remains to be resolved. A more recent generation of simulations (e.g. Cooper et al. 2010b) will also permit more far reaching and robust conclusions.

Funding for SDSS-III has been provided by the Alfred P. Sloan Foundation, the Participating Institutions, the National Science Foundation, and the U.S. Department of Energy. The SDSS-III web site is <http://www.sdss3.org/>.

SDSS-III is managed by the Astrophysical Research Consortium for the Participating Institutions of the SDSS-III Collaboration including the University of Arizona, the Brazilian Participation Group, Brookhaven National Laboratory, University of Cambridge, University of Florida, the French Participation Group, the German Participation Group, the Instituto de Astrofísica de Canarias, the Michigan State/Notre Dame/JINA Participation Group, Johns Hopkins University, Lawrence Berkeley National Laboratory, Max Planck Institute for Astrophysics, New Mexico State University, New York University, the Ohio State University, University of Portsmouth, Princeton University, University of Tokyo, the University of Utah, Vanderbilt University, University of Virginia, University of Washington, and Yale University.

This work was made possible by the support of the Max-Planck-Institute for Astronomy, and was funded by the National Natural Science Foundation of China (NSFC) under Nos. 10821061, 10876040 and 10973021, and supported by the Young Researcher Grant of National Astronomical Observatories, Chinese Academy of Sciences. This work was also supported by the National Basic Research Program of China under grant 2007CB815103.

E. F. B. acknowledges NSF grant AST 1008342.

T.C.B. and Y.S.L. acknowledge partial funding of this work from grants PHY 02-16783 and PHY 08-22648: Physics Frontier Center/Joint Institute for Nuclear Astrophysics (JINA), awarded by the U.S. National Science Foundation.

H. Morrison acknowledges funding of this work from NSF grant AST-0098435.

## REFERENCES

- Abazajian, K., Adelman-McCarthy, J. K., Agüeros, M. A., et al. 2004, *AJ*, 128, 502  
Abazajian, K., Adelman-McCarthy, J. K., Agüeros, M. A., et al. 2005, *AJ*, 129, 1755  
Abazajian, K., Adelman-McCarthy, J. K., Agüeros, M. A., et al. 2003, *AJ*, 126, 2081

- Abazajian, K. N., Adelman-McCarthy, J. K., Agüeros, M. A., et al. 2009, *ApJS*, 182, 543
- Adelman-McCarthy, J. K., Agüeros, M. A., Allam, S. S., et al. 2008, *ApJS*, 175, 297
- Adelman-McCarthy, J. K., Agüeros, M. A., Allam, S. S., et al. 2007, *ApJS*, 172, 634
- Adelman-McCarthy, J. K., Agüeros, M. A., Allam, S. S., et al. 2006, *ApJS*, 162, 38
- Aihara, H., Allende Prieto, C., An, D., et al. 2011, *ApJS*, 193, 29
- Allende Prieto, C., Sivarani, T., Beers, T. C., et al. 2008, *AJ*, 136, 2070
- Bell, E. F., Xue, X. X., Rix, H., Ruhland, C., & Hogg, D. W. 2010, *AJ*, 140, 1850
- Bell, E. F., Zucker, D. B., Belokurov, V., et al. 2008, *ApJ*, 680, 295 [B08]
- Blumenthal, G. R., Faber, S. M., Primack, J. R., & Rees, M. J. 1984, *Nature*, 311, 517
- Bovy, J., Hogg, D. W., & Rix, H. 2009, *ApJ*, 704, 1704
- Bullock, J. S. & Johnston, K. V. 2005, *ApJ*, 635, 931 [BJ05]
- Bullock, J. S., Kravtsov, A. V., & Weinberg, D. H. 2001, *ApJ*, 548, 33
- Carollo, D., Beers, T. C., Chiba, M., et al. 2010, *ApJ*, 712, 692
- Carollo, D., Beers, T. C., Lee, Y. S., et al. 2007, *Nature*, 450, 1020
- Cooper, A. P., Cole, S., Frenk, C. S., & Helmi, A. 2010a, *ArXiv e-prints*
- Cooper, A. P., Cole, S., Frenk, C. S., et al. 2010b, *MNRAS*, 406, 744
- de Jong, J. T. A., Yanny, B., Rix, H., et al. 2010, *ApJ*, 714, 663
- De Propris, R., Harrison, C. D., & Mares, P. J. 2010, *ApJ*, 719, 1582
- Dehnen, W. & Binney, J. J. 1998, *MNRAS*, 298, 387
- Doinidis, S. P. & Beers, T. C. 1989, *ApJ*, 340, L57
- Font, A. S., Johnston, K. V., Bullock, J. S., & Robertson, B. E. 2006, *ApJ*, 646, 886
- Fukugita, M., Ichikawa, T., Gunn, J. E., et al. 1996, *AJ*, 111, 1748
- Gunn, J. E., Carr, M., Rockosi, C., et al. 1998, *AJ*, 116, 3040
- Gunn, J. E., Siegmund, W. A., Mannery, E. J., et al. 2006, *AJ*, 131, 2332



- Hammer, F., Puech, M., Chemin, L., Flores, H., & Lehnert, M. D. 2007, *ApJ*, 662, 322
- Harrigan, M. J., Newberg, H. J., Newberg, L. A., et al. 2010, *MNRAS*, 405, 1796
- Helmi, A., White, S. D. M., de Zeeuw, P. T., & Zhao, H. 1999, *Nature*, 402, 53
- Hogg, D. W., Finkbeiner, D. P., Schlegel, D. J., & Gunn, J. E. 2001, *AJ*, 122, 2129
- Ibata, R., Lewis, G. F., Irwin, M., Totten, E., & Quinn, T. 2001, *ApJ*, 551, 294
- Ibata, R., Martin, N. F., Irwin, M., et al. 2007, *ApJ*, 671, 1591
- Ibata, R. A., Gilmore, G., & Irwin, M. J. 1994, *Nature*, 370, 194
- Ibata, R. A., Gilmore, G., & Irwin, M. J. 1995, *MNRAS*, 277, 781
- Ivezić, Ž., Goldston, J., Finlator, K., et al. 2000, *AJ*, 120, 963
- Ivezić, Ž., Lupton, R. H., Schlegel, D., et al. 2004, *Astronomische Nachrichten*, 325, 583
- Johnston, K. V., Bullock, J. S., Sharma, S., et al. 2008, *ApJ*, 689, 936
- Klement, R., Fuchs, B., & Rix, H. 2008, *ApJ*, 685, 261
- Klement, R., Rix, H., Flynn, C., et al. 2009, *ApJ*, 698, 865
- Koposov, S. E., Rix, H., & Hogg, D. W. 2010, *ApJ*, 712, 260
- Lee, Y. S., Beers, T. C., Sivarani, T., et al. 2008a, *AJ*, 136, 2022
- Lee, Y. S., Beers, T. C., Sivarani, T., et al. 2008b, *AJ*, 136, 2050
- Lynden-Bell, D. & Lynden-Bell, R. M. 1995, *MNRAS*, 275, 429
- Majewski, S. R., Munn, J. A., & Hawley, S. L. 1996, *ApJ*, 459, L73+
- Majewski, S. R., Skrutskie, M. F., Weinberg, M. D., & Ostheimer, J. C. 2003, *ApJ*, 599, 1082
- Morrison, H. L., Helmi, A., Sun, J., et al. 2009, *ApJ*, 694, 130
- Newberg, H. J., Yanny, B., Cole, N., et al. 2007, *ApJ*, 668, 221
- Newberg, H. J., Yanny, B., Rockosi, C., et al. 2002, *ApJ*, 569, 245
- Palma, C., Majewski, S. R., & Johnston, K. V. 2002, *ApJ*, 564, 736

- Pier, J. R., Munn, J. A., Hindsley, R. B., et al. 2003, *AJ*, 125, 1559
- Robertson, B., Bullock, J. S., Font, A. S., Johnston, K. V., & Hernquist, L. 2005, *ApJ*, 632, 872
- Schlaufman, K. C., Rockosi, C. M., Allende Prieto, C., et al. 2009, *ApJ*, 703, 2177
- Searle, L. & Zinn, R. 1978, *ApJ*, 225, 357
- Sharma, S., Bland-Hawthorn, J., Johnston, K. V., & Binney, J. 2011, *ApJ*, 730, 3
- Shen, J., Rich, R. M., Kormendy, J., et al. 2010, *ApJ*, 720, L72
- Sirko, E., Goodman, J., Knapp, G. R., et al. 2004, *AJ*, 127, 899
- Skrutskie, M. F., Cutri, R. M., Stiening, R., et al. 2006, *AJ*, 131, 1163
- Smith, J. A., Tucker, D. L., Kent, S., et al. 2002, *AJ*, 123, 2121
- Smith, M. C., Evans, N. W., Belokurov, V., et al. 2009, *MNRAS*, 399, 1223
- Smolinski, J. P., Lee, Y. S., Beers, T. C., et al. 2011, *AJ*, 141, 89
- Starkenburger, E., Helmi, A., Morrison, H. L., et al. 2009, *ApJ*, 698, 567
- Stoughton, C., Lupton, R. H., Bernardi, M., et al. 2002, *AJ*, 123, 485
- Tucker, D. L., Kent, S., Richmond, M. W., et al. 2006, *Astronomische Nachrichten*, 327, 821
- White, S. D. M. & Rees, M. J. 1978, *MNRAS*, 183, 341
- Xue, X., Rix, H., & Zhao, G. 2009, *Research in Astronomy and Astrophysics*, 9, 1230
- Xue, X. X., Rix, H. W., Zhao, G., et al. 2008, *ApJ*, 684, 1143 [X08]
- Yanny, B., Newberg, H. J., Grebel, E. K., et al. 2003, *ApJ*, 588, 824
- Yanny, B., Newberg, H. J., Johnson, J. A., et al. 2009a, *ApJ*, 700, 1282
- Yanny, B., Newberg, H. J., Kent, S., et al. 2000, *ApJ*, 540, 825
- Yanny, B., Rockosi, C., Newberg, H. J., et al. 2009b, *AJ*, 137, 4377
- York, D. G., Adelman, J., Anderson, Jr., J. E., et al. 2000, *AJ*, 120, 1579

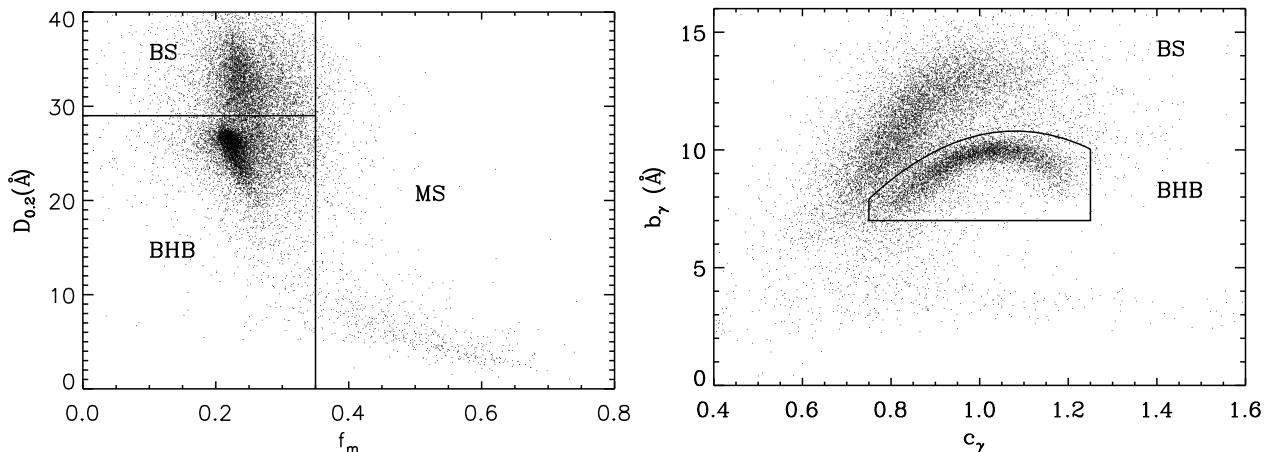


Fig. 1.— BHB star sample selection, based on the Balmer-line shape parameters (see Section 2). The left-hand panel shows the H $\delta$  line parameters  $f_m$  and  $D_{0.2}$ , divided into three regions (following X08 and Sirko et al. 2004): stars with  $f_m > 0.35$  are too cool to be BHB stars – they are likely main-sequence stars; the concentration of stars with  $D_{0.2} > 29\text{\AA}$  is likely due to blue stragglers (BS) with higher surface gravity; the region with  $f_m \leq 0.35$  and  $D_{0.2} \leq 29\text{\AA}$  is used as the BHB selection criterion for the H $\delta$ ,  $D_{0.2}$ , and  $f_m$  method. The right-hand panel shows the H $\gamma$ -line profile parameters  $c_\gamma$  and  $b_\gamma$  for the same stars as in the left panel. Here, BS and BHB stars can be distinguished clearly through their bimodal distribution in this plane. The enclosed region indicates the H $\gamma$  scale width-shape criteria that selects BHB stars. Our BHB sample is composed of all stars satisfying both criteria (left-hand and right-hand panels) simultaneously. This leaves a sample of 4985 objects with a high probability of proper classification as BHB stars (see X08).

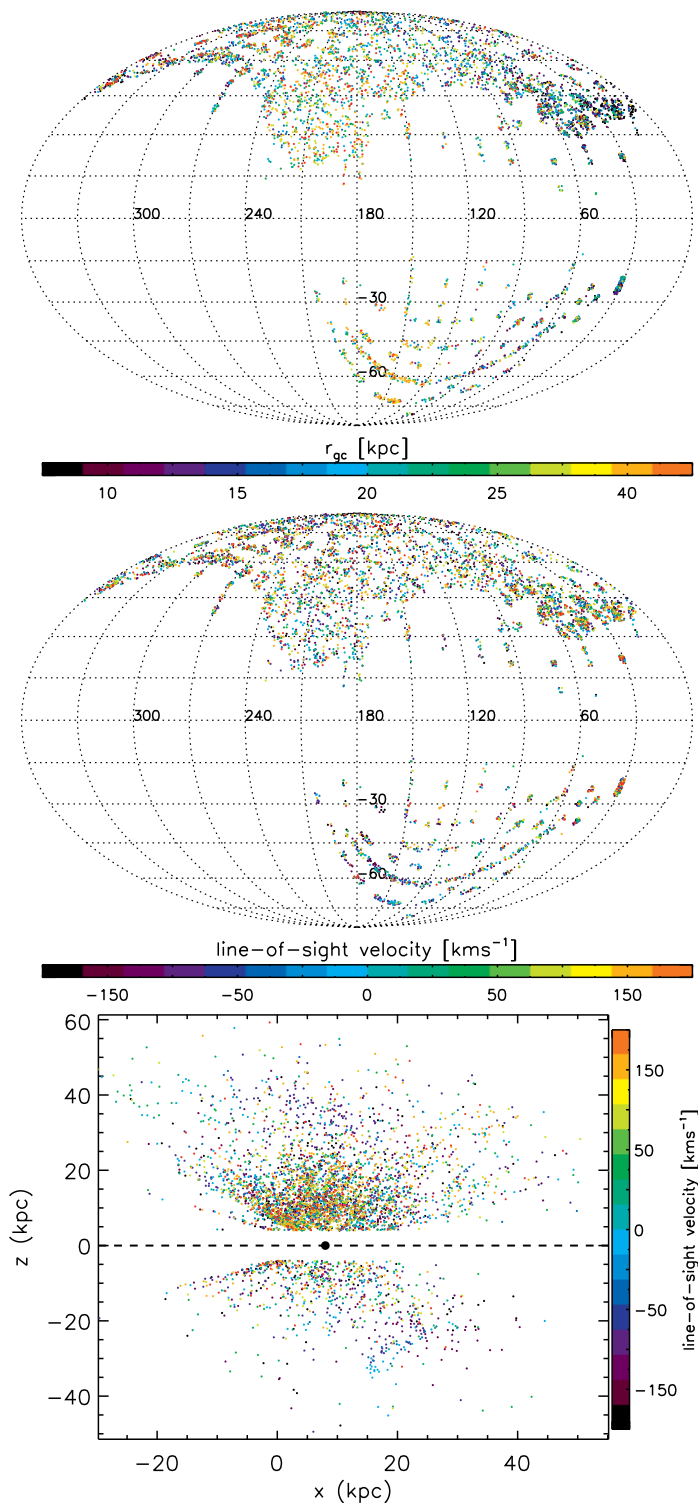


Fig. 2.— Sample properties for the 4625 stars with high probability of being BHB (Figure 1). The first two plots show the Galactic sky coverage of the BHB sample, where stars are colored according to radius and line-of-sight velocity. The spatial distribution ( $x$ - $z$  plane) is shown as the third panel. The coordinate system has its origin at the Galactic center; the large filled circle on the  $x$ - $z$  plot indicates the location of the Sun (8.0 kpc, 0 kpc); and the stars are coded according to line-of-sight velocity.

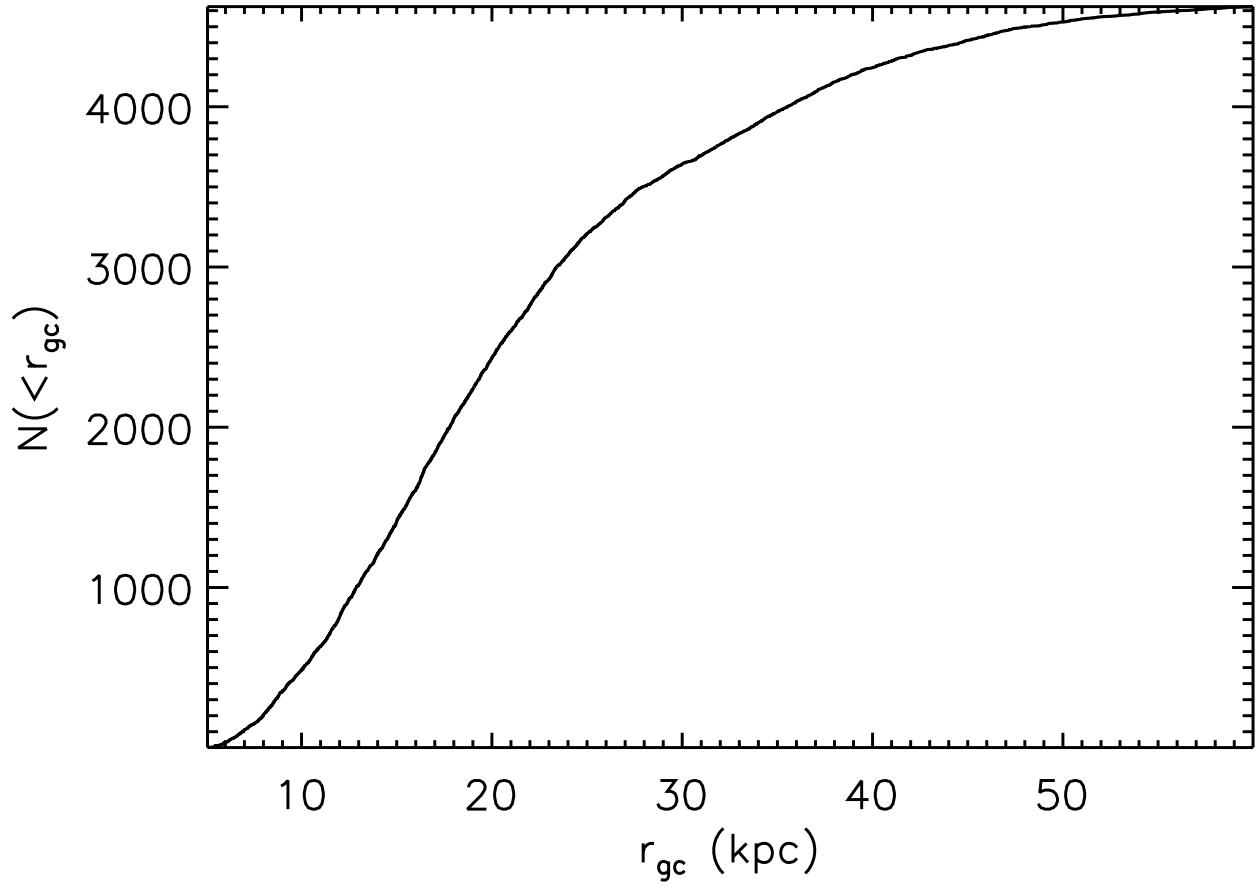


Fig. 3.— The cumulative distribution of BHB stars with distance from the Galactic center,  $r_{gc}$ , with a median distance of 22 kpc. About 90% of the sample lies between 5 kpc and 40 kpc.

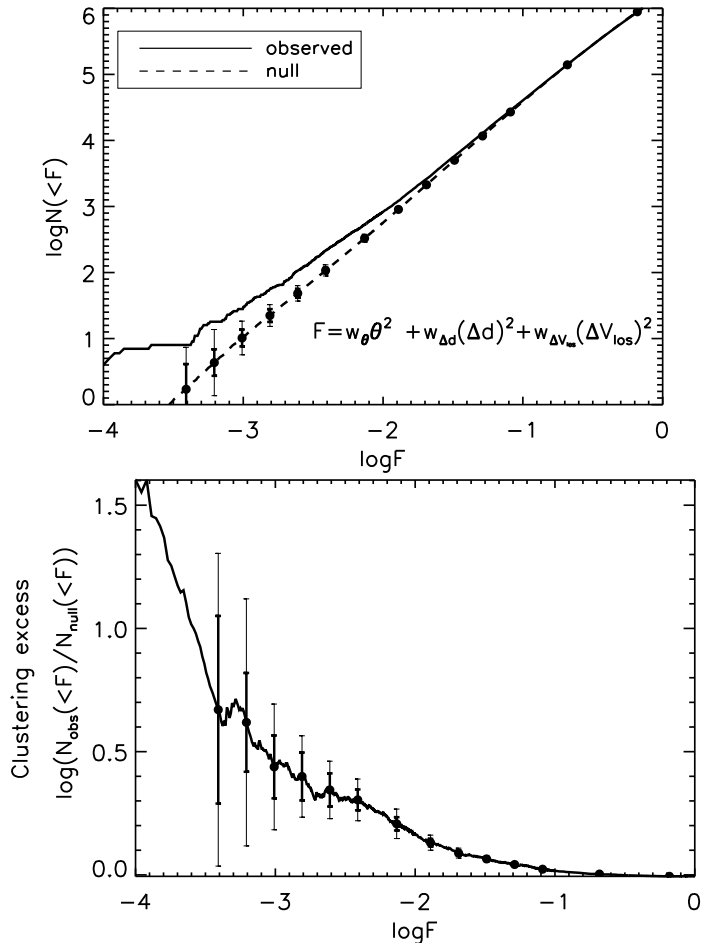


Fig. 4.— (Upper Panel): The close pair distribution,  $N(< F)$ , for the 4243 BHB stars in the SDSS DR8 BHB sample with  $|Z| > 4$  kpc and  $r_{gc} < 40$  kpc.  $F$  is the four-space separation between two BHB stars, taking into account in angle, distance, and line-of-sight velocity (Eq. 1). The solid line is the cumulative distribution of  $F$  as observed; the dashed line is the average cumulative distribution of  $F$  for 100 null hypotheses, where positions, and hence, angular separations for each pair, were retained exactly as in the observations, but distances and line-of-sight velocities were scrambled (see Section 3). The filled circles devote the mean of 100 such null hypotheses; the thick error bars enclose 68% of the distribution, while the thin error bars enclose 95% of the null hypotheses. For small  $F$  one might expect  $N(< F_0) \propto F_0^2$  for the null hypothesis, but the plot shows a somewhat shallower slope, presumably arising from the sparse, but locally dense, angular sampling that results from the widely spaced SEGUE-1/2 spectroscopic plates. (Lower Panel) Ratio of the cumulative distribution, defined as the number of pairs in the BHB sample divided by the average number of null hypotheses below a certain  $F$ ,  $N_{obs}(< F)/N_{null}(< F)$ . The thick and thin error bars are derived from those on upper plot by propagation of error. Both plots demonstrates that there exists a significant excess of close pairs (in distance and velocity) compared to the null hypothesis; BHB stars in our sample clearly exhibit position-velocity substructure.

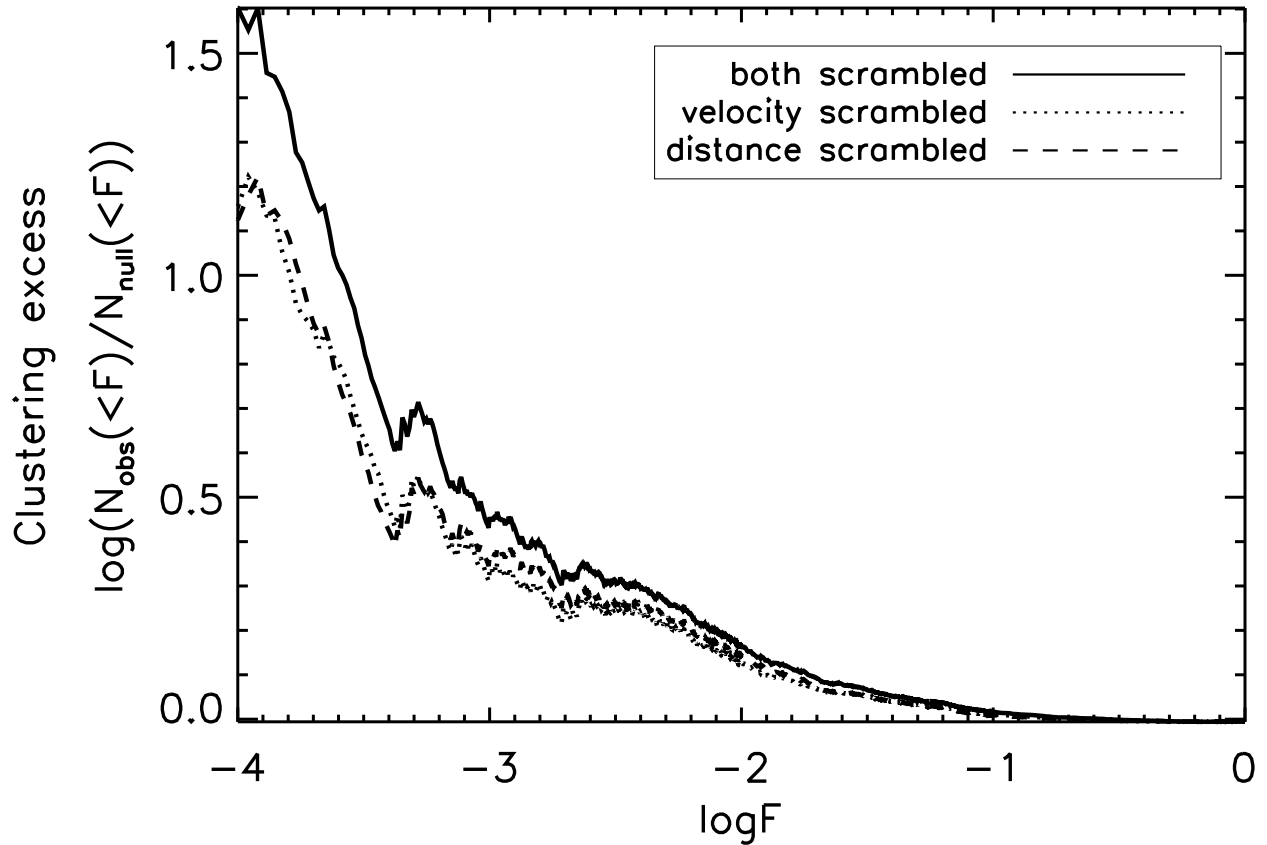


Fig. 5.— The ratio of the cumulative distribution for the BHB sample after either scrambling *only* the distances (dashed line, case I), or *only* the velocities (dotted line, case II), or both of them (solid line, case III). In cases I and II an excess of close pairs is observed at a comparable level, but is weaker than that of case III. This implies that the substructure signal arises in comparable parts from both the distance and the line-of-sight velocity domains.

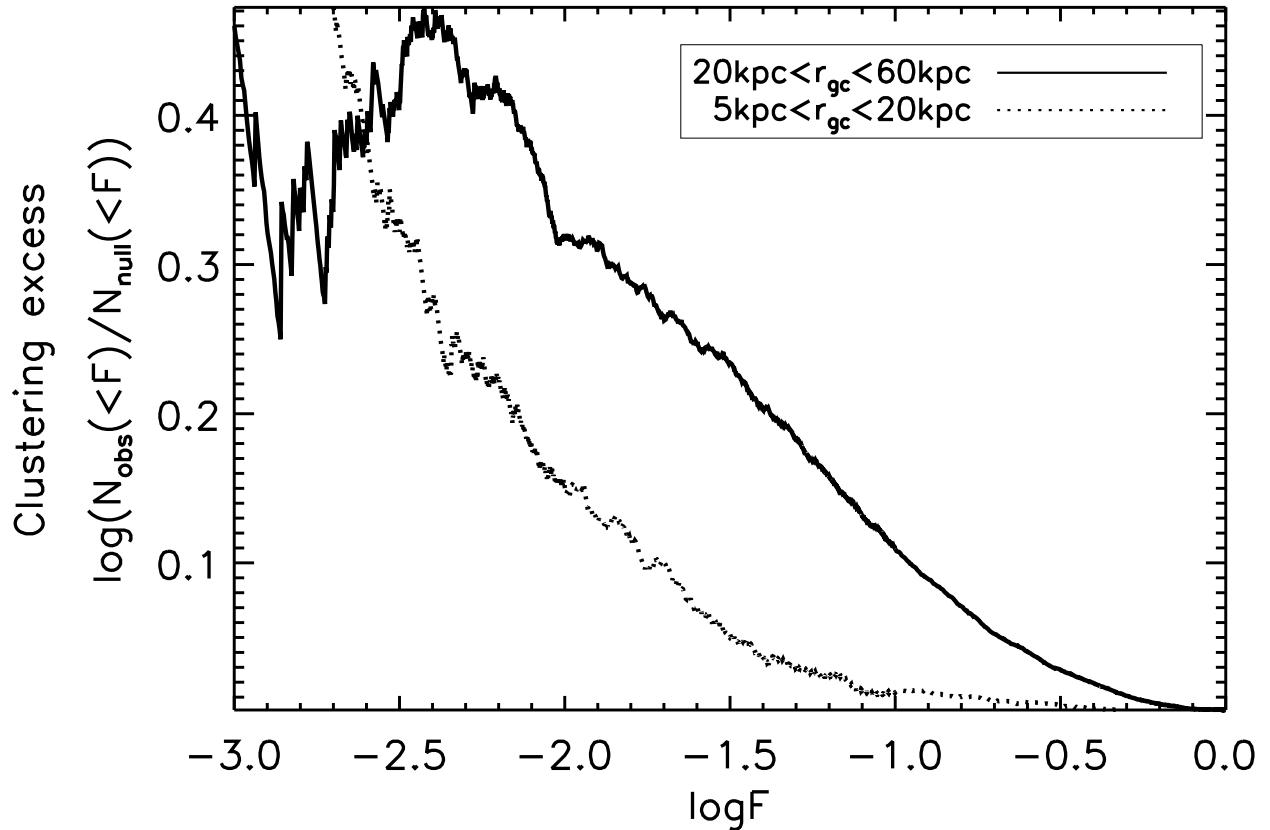


Fig. 6.— The ratio of the cumulative distribution of  $F$  for BHB stars in two broad Galactocentric distance ranges: subsample I, which covers  $5 \text{ kpc} < r_{\text{gc}} < 20 \text{ kpc}$  (dotted line), subsample II, which covers  $20 \text{ kpc} < r_{\text{gc}} < 60 \text{ kpc}$  (solid line). The excess of close pairs is observed in both subsamples. The plot illustrates that a position-velocity substructure signal is present in both distance ranges, covering the inner and outer stellar halo, and the substructure signal is more pronounced at large radii.



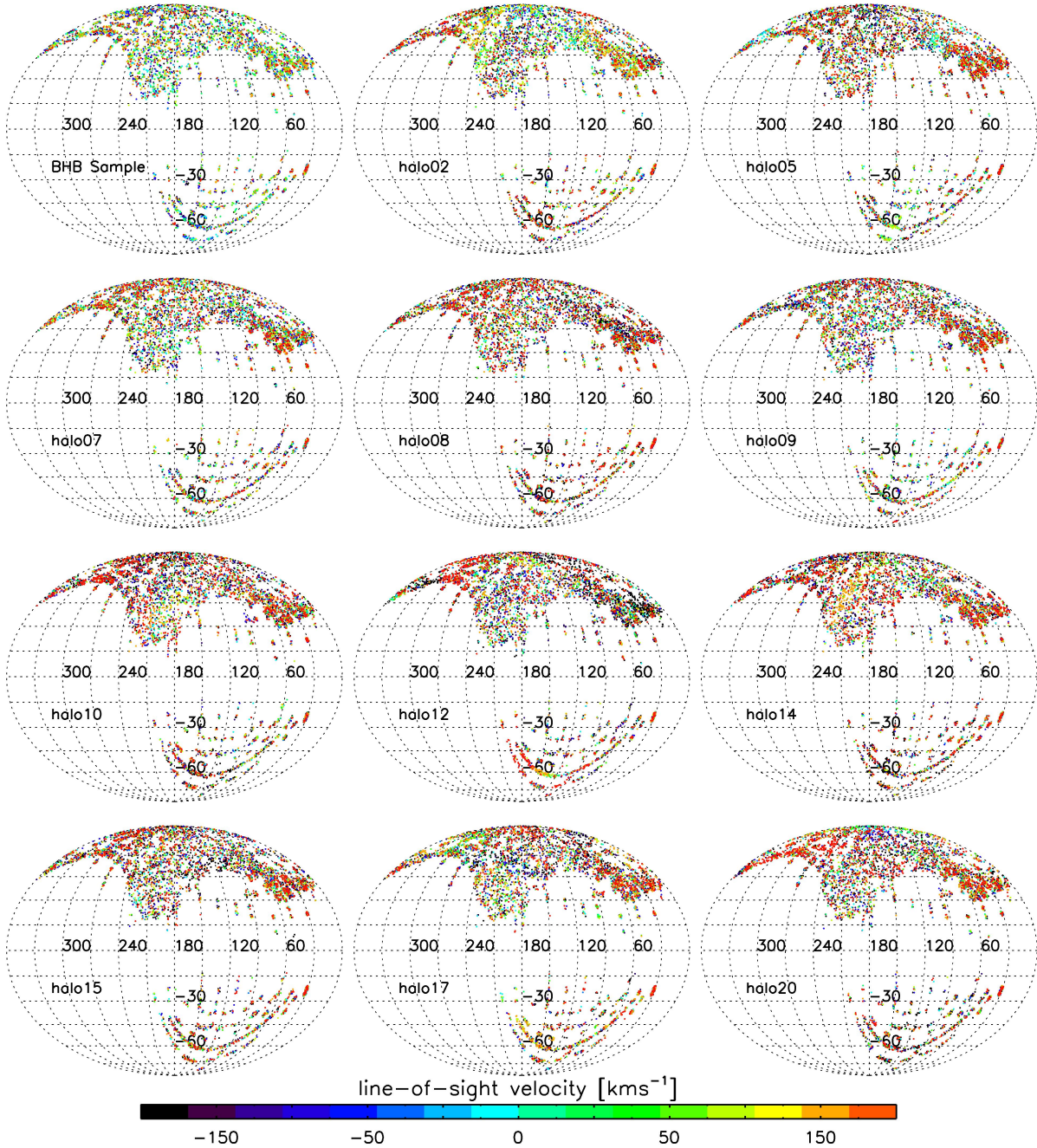


Fig. 7.— The sky coverage for the BHB sample and 11 mock-observations from BJ05. The simulations were sampled in angular coverage and distance distribution to resemble the actual BHB sample. The stars are coded according to line-of-sight velocity. This figure shows that the velocity distributions between observation and the simulations differ somewhat. There are more stars with  $|V_{\text{los}}| > 250\text{kms}^{-1}$  in the simulations.

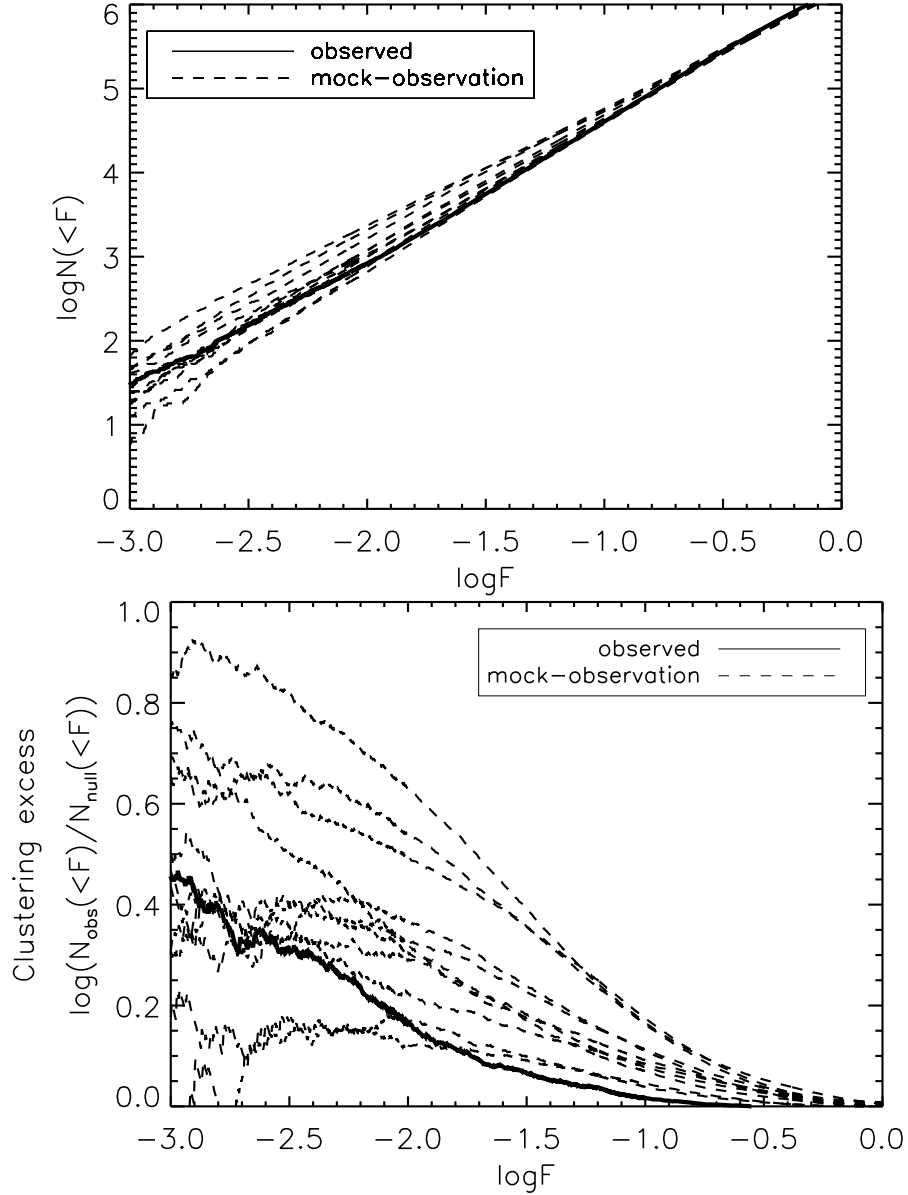


Fig. 8.— The upper panel is the close pair distribution for the observed BHB sample and the 11 simulations. The solid line is the cumulative distribution of  $F$  for the observed BHB sample; the dashed lines are the  $F$  distributions for the mock-observations of the 11 simulations. Overall, the observations fall well within the range of expectation from the BJ05 simulations, but the simulations have somewhat more mid-scale power ( $\log F \sim -2.5$  to  $-1$ ) than the observations. The lower panel shows the data-model comparison for the position-velocity substructure. We show the ratio of the cumulative distribution for observations (solid line) and 11 mock-observations from BJ05 (dashed lines). This figure shows that all simulations exhibit position-velocity clustering as an excess of  $N_{obs}(<F)$  for small  $F$ . The observed ratio of the cumulative distribution is smaller than most of those seen in the simulations, where the halo is exclusively made up from disrupted satellites.

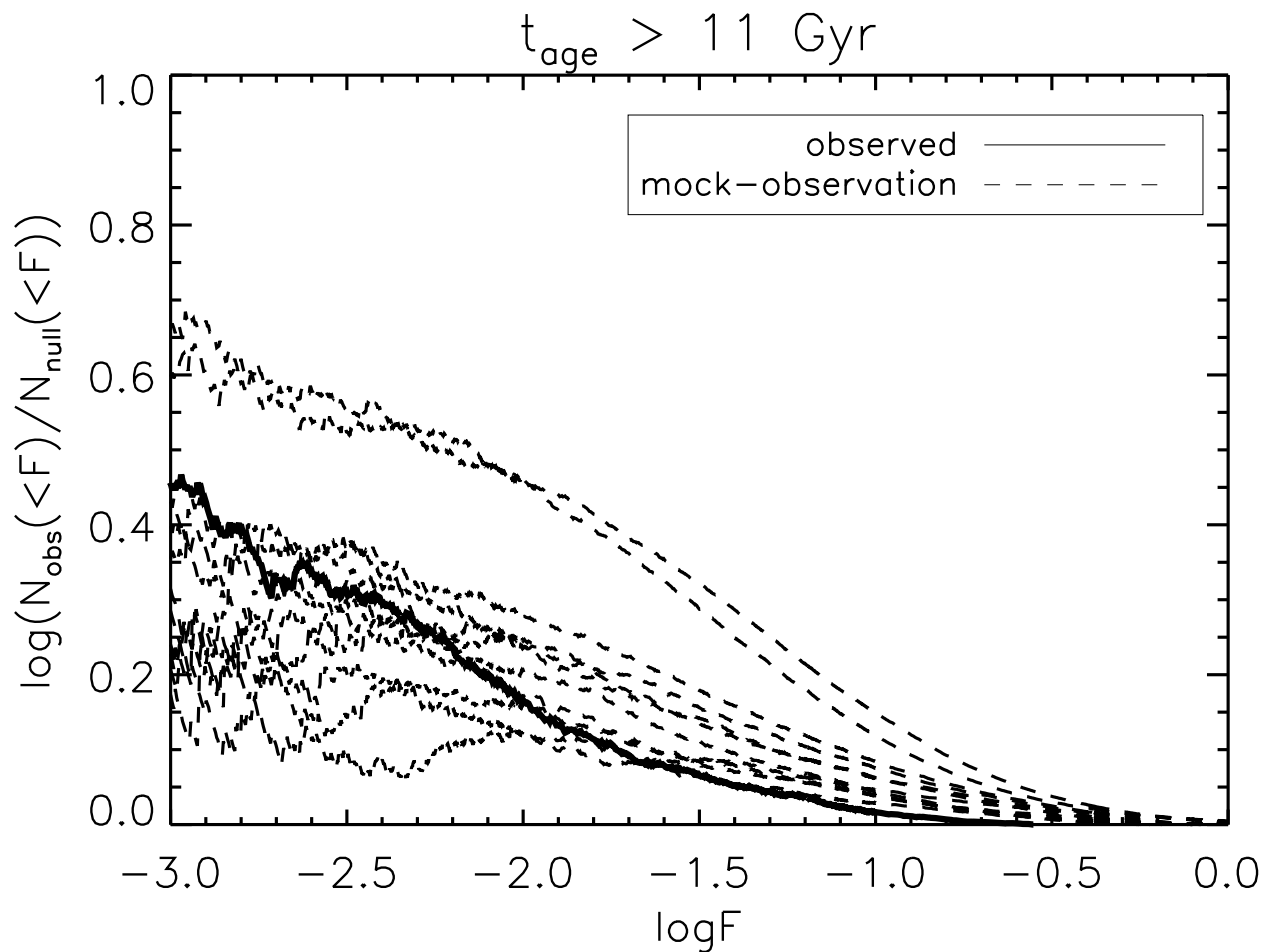


Fig. 9.— The ratio of the cumulative distributions for the BHB sample and particles older than 11 Gyr in each of the 11 BJ05 simulations. The solid lines are the ratio of the cumulative distributions for the observation and the dashed lines are the ratios of the cumulative distributions for the 11 mock-observations. Clearly, the observation is comparable to the older parts of most simulations (except 2 BJ05 halos).

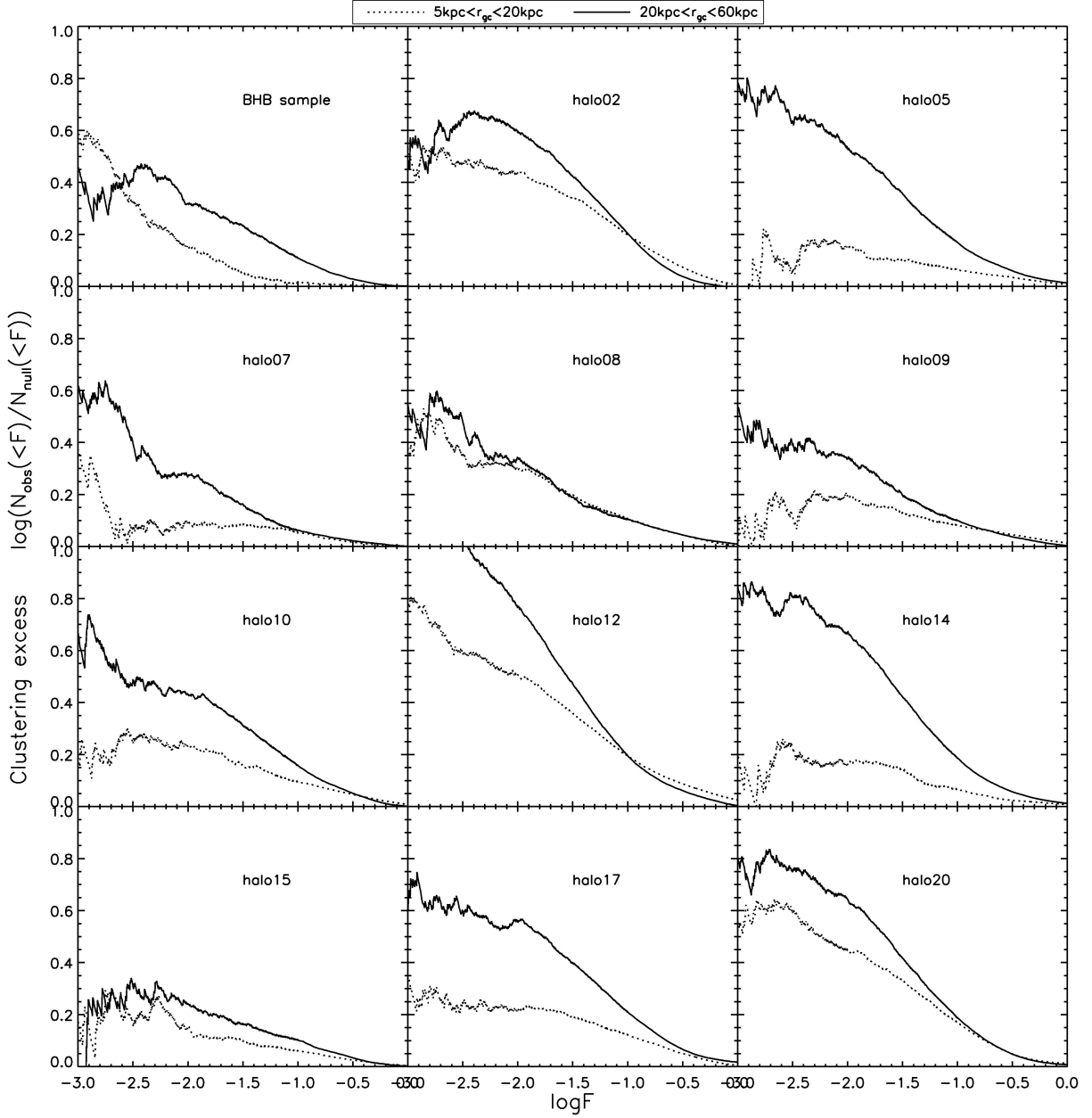


Fig. 10.— The ratio of the cumulative distributions for BHB stars and the 11 BJ05 simulations in regions that should be dominated by the outer-halo (subsample II:  $20 \text{ kpc} < r_{gc} < 60 \text{ kpc}$ ; solid lines) and the inner-halo (subsample I:  $5 \text{ kpc} < r_{gc} < 20 \text{ kpc}$ ; dotted lines) populations, respectively. The figure shows that the outer halo exhibits a more pronounced substructure signal than the inner halo for most simulations.

Table 1. List of 4985 BHB stars selected from SDSS DR8

SpName	RA degree	Dec degree	l degree	b degree	g mag	u - g mag	g - r mag	$D_{0.2,\delta}$ Å	$f_{m,\delta}$ --	$c_\gamma$ --	$b_\gamma$ Å	d kpc	r kpc	x kpc	y kpc	z kpc	HRV km s <sup>-1</sup>	HRVerr km s <sup>-1</sup>	RVgal km s <sup>-1</sup>
3141-55008-498	331.047394	6.292428	66.235764	-37.543682	18.94	1.19	-0.07	22.86	0.25	0.86	9.17	46.6	44.7	-6.9	-33.8	-28.4	-115.8	7.7	46.4
3141-55008-477	330.606934	6.429413	66.000389	-37.124928	16.96	1.21	-0.12	26.30	0.23	0.93	9.65	19.1	18.2	1.8	-13.9	-11.6	-121.4	2.0	41.5
3141-55008-454	330.924957	7.108576	66.898819	-36.909523	17.05	1.16	-0.14	27.42	0.20	0.94	9.45	20.0	19.1	1.7	-14.7	-12.0	-275.2	2.3	-110.8
3141-55008-449	330.812134	7.425377	67.099251	-36.614384	16.05	1.14	-0.17	26.18	0.22	1.06	9.72	12.6	12.6	4.1	-9.3	-7.5	4.8	1.3	170.1
3141-55008-432	330.167633	6.321596	65.538742	-36.867428	18.35	1.25	-0.14	25.37	0.16	0.97	9.92	36.4	34.6	-4.1	-26.5	-21.8	-159.2	4.7	3.8
3141-55008-419	330.375885	7.419462	66.734512	-36.296391	16.39	1.21	-0.06	22.91	0.20	0.90	8.33	14.4	14.1	3.4	-10.6	-8.5	-171.1	1.9	-5.4
3141-55008-401	330.380737	7.128237	66.468353	-36.493710	19.12	1.24	-0.09	25.80	0.32	0.98	9.59	51.8	49.8	-8.6	-38.2	-30.8	-302.2	10.2	-137.3
3141-55008-365	330.155487	7.230328	66.379021	-36.258785	16.51	1.18	-0.05	23.00	0.22	0.83	7.67	15.2	14.7	3.1	-11.2	-9.0	-185.1	1.8	-19.8
3141-55008-200	330.074493	5.726783	64.899216	-37.186333	17.73	1.19	-0.10	25.55	0.27	0.89	9.19	27.3	25.7	-1.2	-19.7	-16.5	-187.9	3.3	-26.4
3141-55008-097	330.798920	5.458101	65.236534	-37.907768	17.17	1.17	-0.15	27.41	0.24	1.01	10.44	21.1	20.0	1.0	-15.1	-13.0	-29.2	2.5	131.0
3478-55008-051	241.184311	35.821747	57.356461	48.304852	16.45	1.16	-0.18	24.60	0.21	1.02	9.84	15.2	14.4	2.6	-8.5	11.3	-281.2	2.8	-146.1

Note. — The first column are object name composed by plate-MJD-fiberID and the next four columns contains the astrometry (ra, dec, l, b) for each object. The magnitude and color are in the next four columns: corrected for extinction. The next four columns are the linewidth parameters from the Balmer lines. The positions are listed in the next five columns. The radial velocities and errors are listed next. The complete version of this table is in the electronic edition of the Journal. The printed edition contains only a sample.